Role of nanoscopic liquid bridges in static friction

Henry Bock,* Dennis J. Diestler,† and Martin Schoen‡
Stranski-Laboratorium für Physikalische und Theoretische Chemie, Institut für Chemie, Sekretariat TC 7, Technische Universität Berlin, Straße des 17. Juni 124, D-10623 Berlin, Germany
(Received 23 February 2001; published 25 September 2001)

Interpretations of recent experiments on the effects of humidity on friction hypothesize that liquid-water bridges can span nanoscopic gaps at the interface between the sliding surfaces. By means of a lattice-gas model the mechanisms by which such bridges may engender static friction at a single ideal nanoscopic contact were studied. The model contact consists of a simple (spherically symmetric) fluid constrained between two plane-parallel substrates decorated with weakly and strongly attractive stripes that alternate periodically in one transverse direction. In analogy with the experiments the shear yield stress (yield strength) τ_s of the contact was computed as a function of the chemical potential μ of the fluid (the analog of humidity). The influence of other thermodynamic state variables, such as temperature and distance between the substrates, and of the relative strength of the stripes on the yield-strength curves (i.e., τ_s versus μ) was explored. Some intriguing correlations between experiment and theory are observed.

DOI: 10.1103/PhysRevE.64.046124 PACS number(s): 81.40.Pq, 61.46.+w, 62.25.+g, 68.55.−a

I. INTRODUCTION

The force of static friction F_s between macroscopic bodies in contact, taken to be the minimum (shear) force needed just to initiate relative movement of the bodies parallel with the plane of contact (interface), is usually observed to be proportional via the coefficient of static friction μ_s to the force normal to the interface F_n (i.e., Amonton's law) [1], that is,

$$F_s = \mu_s F_n . \tag{1}$$

As two unlubricated macroscopic surfaces are pressed together, they make *molecular* contact at relatively few asperities (spatially irregular prominences) of microscopic dimension [2]. The entire load F_n is borne by these asperities, which may therefore undergo relaxations (e.g., plastic flow) that are slow on the time scale of the measurement of F_s. As a result, μ_s is often observed to depend on the time of aging (i.e., the time elapsed between the measurement of F_s and the contacting of the surfaces, or, more generally, the initialization of the system). For example, in a definitive study of paper sliding on paper Heslot *et al.* [3] observed a logarithmic dependence of μ_s on time,

$$\mu_s(t) = a_s + b_s \ln(t), \tag{2}$$

where a_s and b_s are constants and t is the time of aging. Heslot *et al.* [3] imputed this aging to the ''creeping'' of asperities. Similar behavior was found for steel sliding on soft metals [4] and for rock sliding on rock [5,6]. The aging phenomenon is also observed in mechanical brakes and clutches, where a monotonic increase in the coefficient of friction with time (see, for example, Fig. 4 in [7]) is correlated with the chemical composition at the interface.

Although the surfaces in the above mentioned experiments are dry, in the sense that they are not lubricated, they are nevertheless exposed to (generally uncontrolled) ambient atmospheres. The possible role of adsorption at the interface must therefore be considered. Bocquet *et al.* [8] studied the effect of humidity on the mechanical behavior of an ideal granular medium (spherical glass beads contained in a cylindrical drum). They found that, when the humidity is sufficiently high, the angle of first avalanche of the beads, which corresponds to the condition in which the shear stress at the bead-bead contact *locally* just exceeds the static friction F_s (or shear yield stress τ_s), depends logarithmically on the time elapsed after an initial rolling of the drum is ceased. In a more recent study of the mechanical properties of the glass-bead medium, D'Anna [9] also observed a logarithmic dependence on aging time. Indeed, Bocquet *et al.* [8] aver that the logarithmic character is universal and they hypothesize that it is due to the formation of nanoscopic liquid water bridges that span interfacial gaps. They assume that bridge formation results from capillary condensation, which they treat as a thermally activated process obeying Arrhenius' law [10,11], with an activation energy proportional to the logarithm of the relative humidity. A key assumption upon which the logarithmic form Eq. (2) ultimately rests is that there exists a distribution of widths of interfacial gaps that can serve as sites for nucleation of bridges, so that at any given aging time only a fraction of the gaps are bridged. The model also assumes that the classical empirical relation Eq. (1) holds at the level of the gaps, where now μ_s is the *constant* ''internal'' friction coefficient. The increase in yield stress with time is due solely to the increase in the fraction of the interfacial area covered by bridges, which are under tension, according to Kelvin's equation [12], which is assumed to apply.

Although the above described aging experiments were carried out at the macroscopic scale, their interpretation appeals to the existence of particular nanoscopic entities (liquid

*Electronic address: henry@terra.chem.tu-berlin.de
†Permanent address: Department of Agronomy and Horticulture, University of Nebraska–Lincoln, Lincoln, NE 68583–0915. Electronic address: ddiestler1@unl.edu
‡Electronic address: martin@terra.chem.tu-berlin.de

bridges) whose behavior is dubiously related to the experimental conditions (the relative humidity) by Kelvin's equation. Being based on classical thermodynamics, the model of Bocquet *et al.* [8] can provide no information on the *molecular* origin of friction or on the mechanisms by which liquid bridges affect F_s. In particular, the coupling between the molecular scale structure of the bridges and the nanoscale geometrical and chemical variations in the asperities must significantly influence the behavior of the bridges. In view of the important part played by nanoscopic liquid bridges in such practical phenomena as granular flow [8,9] and geological transformations [5,6], and in anticipation of the crucial role of bridges in the functioning of microdevices [13,14], it behooves one to investigate the bridges on their own length scale. For this purpose it is necessary to study single, well defined nanoscopic asperities. In recent years a variety of techniques, including lithography [15], wet chemical etching [16], and microcontact printing [17], have been used to fabricate solid substrates possessing precise geometrical or chemical patterns on micro- to nanoscales. Such decorated substrates can be moved over each other with almost atomic precision in regulated atmospheres, say, by means of surface force apparatus [18] or the atomic force microscope [19–21]. This experimental setup would permit the investigation of frictional behavior (in particular, the role of liquid bridges) of idealized contacts directly on the molecular scale. Indeed, atomic force microscopy has already been used to explore the effects of bridge formation on adhesion [22] and on friction [23,24], albeit for macroscopic, unpatterned substrates.

In light of the feasibility of direct experimental study of liquid bridges at the nanoscale, we have undertaken a parallel computational investigation of an idealized nanoscopic contact: a film confined between plane-parallel substrates consisting of periodically alternating weakly and strongly (attractive) adsorbing strips. This model satisfies the minimum requirement for the contact to be capable of sustaining a shear stress: heterogeneity in directions parallel with the interface. We have previously studied the prototype using both the (discrete) mean-field lattice-gas approximation [25–28] and the Monte Carlo method in a specialized isostress-isostrain ensemble for a model with continuous intermolecular interaction potentials [26,29,30]. In prior work we were concerned mainly with the phase behavior of the adsorbed film. Indeed, the occurrence of liquid bridges spanning the gaps between attractive strips in opposing substrates was confirmed. (We note that Röcken and Tarazona [31] were apparently the first to report the existence of bridge phases observed in a lattice-gas treatment of a similar model.) The effects of shearing on the phase diagram were also examined [25–28]. Since the lattice-gas model exhibits the essential features of the shearing behavior of the prototypical contact, as confirmed by Monte Carlo simulations [26], and since it is less demanding computationally than the Monte Carlo method, we shall adopt it for our present purpose.

In Sec. II we describe the model contact and its treatment within the framework of the mean-field lattice-gas approximation. The principal results of the computations, the yield-strength curves (i.e., τ_s versus chemical potential μ), are presented in Sec. III. The influence on the yield-strength curve of selected parameters of the model is explored. Section IV is given to a summary of our findings and to correlations between results of the calculations and the results of the experiment of Scherge *et al.* [23].

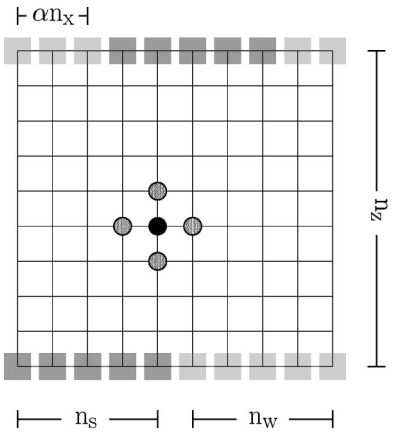

FIG. 1. Schematic side view of model contact: simple-cubic lattice gas confined between two plane-parallel substrates consisting of strongly attractive stripes alternating with weakly attractive ones periodically in the x direction. A molecule at a site in the central region (black circle) interacts only with its six nearest neighbors (the four in the x-z plane are depicted as light gray circles; the two additional ones in the y-z plane are not shown). At n_s sites on either substrate (dark gray squares) a molecule is subject to the ''strong'' stripe ($\Phi_i = -\epsilon_{fs}$) as well as to up to five nearest neighbors; at n_w sites (light gray squares) a molecule is subject to the ''weak'' stripe ($\Phi_i = -\epsilon_{fw}$) plus up to five nearest neighbors.

II. MODEL AND THEORY

The idealized contact consists of a simple fluid (film) confined between two plane-parallel substrates decorated with strongly and weakly attractive chemical stripes that alternate periodically in one transverse (x) direction. We take the chemical stripes to lie parallel with the y axis, so that the film is homogeneous (and its properties are therefore translationally invariant) in the y direction. We treat the film within the mean-field lattice-gas approximation, as detailed in previous articles [25–28]. The positions of film molecules are constrained to the sites of an $n_x \times n_y \times n_z$ simple-cubic lattice that spans the gap between the substrates. Space is thus discretized and distance is measured in units of the lattice constant ℓ, taken to be infinitesimally larger than the diameter of a film molecule. On account of the hard-core repulsion, at most only one film molecule can occupy a lattice site. Figure 1 schematizes a single unit cell of the contact projected onto the x-z plane. The ''weak'' and ''strong'' stripes span a total of n_w ($=5$, as depicted in Fig. 1) and n_s ($=5$) lattice sites in the x direction. We assume that the substrates can be displaced relative to each other in the x and z directions by only integral numbers of sites (since space is discrete). The relative alignment of the substrates in the x direction is specified by the registry α, which is defined as $\alpha \equiv \Delta n_x / n_x$, where Δn_x is the number of sites by which the substrates are out of ''exact'' registry ($\alpha = 0$, which is taken to be where stripes of like type are precisely opposite each other).

We assume that the configurational energy can be expressed as a sum of interactions between nearest-neighbor pairs of molecules. We take the substrates to be so far apart that their direct interaction is negligible. The interaction between film molecules is described by a square-well potential having an attractive well of width ℓ and depth ϵ_{ff}. The restriction on the occupancy of a site to a single molecule implicitly accounts for the repulsive part of the square well. The internal energy of the system can therefore be written in the mean-field approximation as

$$\mathcal{U}[\boldsymbol{\rho}]=-\frac{\epsilon_{ff}}{2}\sum_{i}^{\mathcal{N}}\sum_{j}^{\nu(i)}\rho_i\rho_j+\sum_{i}^{\mathcal{N}}\Phi_i\rho_i, \tag{3}$$

where $\boldsymbol{\rho}=\{\rho_1,\rho_2,\ldots,\rho_{\mathcal{N}}\}$ is a vector whose elements are the (*a priori*) unknown mean occupation numbers (i.e., densities), $\mathcal{N}=n_x n_y n_z$ is the number of sites, and $\nu(i)$ is the number of nearest neighbors of site i ($\nu=5$ or 6 in three dimensions). In Eq. (3), $\Phi_i=\Phi_i^{[1]}+\Phi_i^{[2]}$ stands for the film-substrate potential, where

$$\Phi_i^{[1]}\equiv\Phi^{[1]}(x_i,z_i)=\begin{cases}\infty, & z_i<1\\ \left.\begin{matrix}-\epsilon_{fs}, 1\leqslant x_i\leqslant n_s\\ -\epsilon_{fw}, n_s<x_i\leqslant n_x\end{matrix}\right\}, & z_i=1\\ 0, & z_i>1\end{cases} \tag{4}$$

represents the interaction with the lower substrate. Likewise,

$$\Phi_i^{[2]}\equiv\Phi^{[2]}(x_i,z_i)=\begin{cases}\Phi^{[1]}(x_i-\alpha n_x,n_z+1-z_i), & \alpha n_x<x_i\leqslant n_x\\ \Phi^{[1]}[x_i-n_x(\alpha-1),n_z+1-z_i], & 0<x_i\leqslant\alpha n_x\end{cases} \tag{5}$$

specifies the interaction with the upper substrate where lattice sites are restricted to the set $\{(x_i,z_i)|1\leqslant x_i\leqslant n_x,1\leqslant z_i\leqslant n_z\}$ (see Fig. 1).

We take the relative motion of the substrates to be sufficiently slow that the film remains in thermodynamic equilibrium at all instants. That is, we regard sliding as a reversible (quasistatic) process and apply equilibrium statistical mechanics to compute the properties of the system. We note that the sliding of real contacts is generally irreversible (hysteretic) to an extent that depends on the time of measurement t_m (proportional to the reciprocal of the rate of change of α, or equivalently the shear rate) relative to the relaxation time t_r of the rate-limiting molecular process involved in the creation and destruction of the liquid bridges. In essence we assume $t_m\gg t_r$.

We treat the lattice gas as an open system in the usual thermodynamic sense so that its thermodynamic state is specified by temperature T and chemical potential μ. Thus, in thermodynamic equilibrium the grand potential Ω of the lattice is minimum for a given set $\{T,\mu\}$. An upper bound on Ω is given by the grand-potential functional $\Omega[\boldsymbol{\rho}]$ [28],

$$\Omega[\boldsymbol{\rho},T,\mu]=k_BT\sum_{i}^{\mathcal{N}}[\rho_i\ln\rho_i+(1-\rho_i)\ln(1-\rho_i)]+\mathcal{U}[\boldsymbol{\rho}]-\mu\sum_{i}^{\mathcal{N}}\rho_i. \tag{6}$$

The local density (vector) $\boldsymbol{\rho}$ is determined by minimizing Ω through the iterative procedure detailed in Ref. [26]. Substitution of the resulting $\boldsymbol{\rho}$ back into the functional expression on the right side of Eq. (6) yields the approximate value of the grand potential. Note that $\Omega[\boldsymbol{\rho}]$ is an implicit function of eight parameters: ϵ_{fs}, ϵ_{fw}, n_s, and n_w, which specify the chemical decoration of the substrates; αn_x and n_z, respectively the registry and distance between the substrates; T and μ. Because the contact is homogeneous in the y direction, the dependence of $\Omega[\boldsymbol{\rho}]$ on n_y is trivial (that is, $\Omega[\boldsymbol{\rho}]$ is a homogeneous function of degree 1 in n_y, all other parameters being fixed).

The thermodynamic property of primary interest in the present context is the shear stress T_{zx}, which can be expressed in general as the rate of change of Ω with the registry per unit contact area [26]. Within the framework of the discrete lattice model, we approximate T_{zx} by the central-difference formula

$$T_{zx}(\alpha n_x)\simeq\frac{1}{2n_xn_y}[\Omega(\alpha n_x+1)-\Omega(\alpha n_x-1)]. \tag{7}$$

III. RESULTS

The object of principal interest is the shear *yield* stress τ_s of the model contact or, equivalently, the force of static friction $F_s=\tau_sA$, where $A=n_xn_y$ is the area of the contact and

$$\tau_s(T,\mu)=\max_{\alpha n_x}T_{zx}(\alpha n_x;T,\mu) \tag{8}$$

is the maximum shear stress T_{zx} that can be sustained by the contact as the substrates are slid over one period in the x direction while other thermodynamic state variables (μ, T, and n_z) are held fixed. In particular, we focus on τ_s as a function of μ with other parameters (except αn_x) kept constant. The dependence of τ_s on μ is the analog of the dependence of friction on humidity, as measured, for example, in the experiment of Scherge *et al.* [23]. The chemical potential of the *bulk* vapor relative to its value at saturation, $\mu/\mu^{\rm sat}$, (where $\mu^{\rm sat}=-3\epsilon_{ff}$ independent of T in the case of the cubic lattice model employed here) is proportional to the logarithm of the relative ''humidity'' (i.e., to $\ln[p/p^{\rm sat}(T)]$, where p is the vapor pressure, less than the pressure $p^{\rm sat}(T)$ of the saturated vapor).

Despite the relative simplicity of the present model, the phase behavior of the confined lattice gas is quite rich, as was demonstrated recently [28]. However, with increasing T most phases, except the gas, liquid, and bridge, become metastable or unstable at temperatures below those considered here. Of thesethree principal phases only the bridge can support a non-negligible shear stress. A bridge phase consists of a high(er)-density region stabilized by the ''strongly'' at-

TABLE I. Values of varied parameters (in dimensionless units defined in text). In all cases $\epsilon_{fs}=2.0$, $n_s=n_w=20$.

Case	ϵ_{fw}	n_z	T
I	0.5	5	1.2
II	0.5	10	1.2
III	0.0	10	1.2
IV	0.0	10	1.35

tractive stripe (n_s, ϵ_{fs}) surrounded by two low(er)-density regions supported predominantly by the ''weakly'' attractive stripe (n_w, ϵ_{fw}). High(er)- and low(er)-density regions of bridge phases alternate periodically in the x direction. Thus, a bridge phase is inhomogeneous in the z direction on account of mere confinement; it is also inhomogeneous in the x direction on account of the chemical corrugation. It is this latter inhomogeneity that enables bridge phases to sustain a shear stress applied in the x direction [26].

However, the range of values of μ over which bridges can exist is more or less restricted, depending on the values of the other parameters. Moreover, the eight-dimensional space of parameters is rather large, even though the model is one of the simplest capable of exhibiting bridge phases. To keep the computational burden within manageable bounds, we arbitrarily fix the relative strength of the ''strong'' stripe (ϵ_{fs}) and the x dimensions of the stripes (n_s and n_w) and look at the influence of only ϵ_{fw}, n_z, and T on plots of τ_s versus μ, to which we refer henceforth as yield-strength curves.

Table I lists the values of the parameters for each of the four particular cases considered here. All numerical values are henceforth given in standard dimensionless units (i.e., length in units of the lattice constant ℓ, energy in units of the depth ϵ_{ff} of the fluid-fluid square well, stress (pressure) in units of $\epsilon_{ff}\ell^{-3}$, and temperature in units of ϵ_{ff}/k_B, where k_B is Boltzmann's constant).

A. Thermodynamic stability of bridge phases

Figure 2 illustrates the impact of a shear strain αn_x on the phase behavior of bridge phases under various conditions (see Table I). Consider, for example, the curve labeled I in Fig. 2(a). It consists of two branches at lower and higher chemical potentials, which merge at $\alpha n_x=20$. The lower branch represents the coexistence line $\mu_x^{gb}(T,\alpha n_x)$, that is, the chemical potential at which gas (g) and bridge (b) phases coexist for a given T and αn_x. Likewise, the upper branch $\mu_x^{bl}(T,\alpha n_x)$ represents the chemical potential of coexisting bridge and liquid phases. The branches merge at $\alpha_> n_x$, which is defined through

$$\mu_x^{gb}(T,\alpha_> n_x)=\mu_x^{bl}(T,\alpha_> n_x). \tag{9}$$

According to the principles of equilibrium thermodynamics, $\mu_x^{ij}(T,\alpha n_x)$ is determined via

$$\Omega^i=\Omega^j, \tag{10}$$

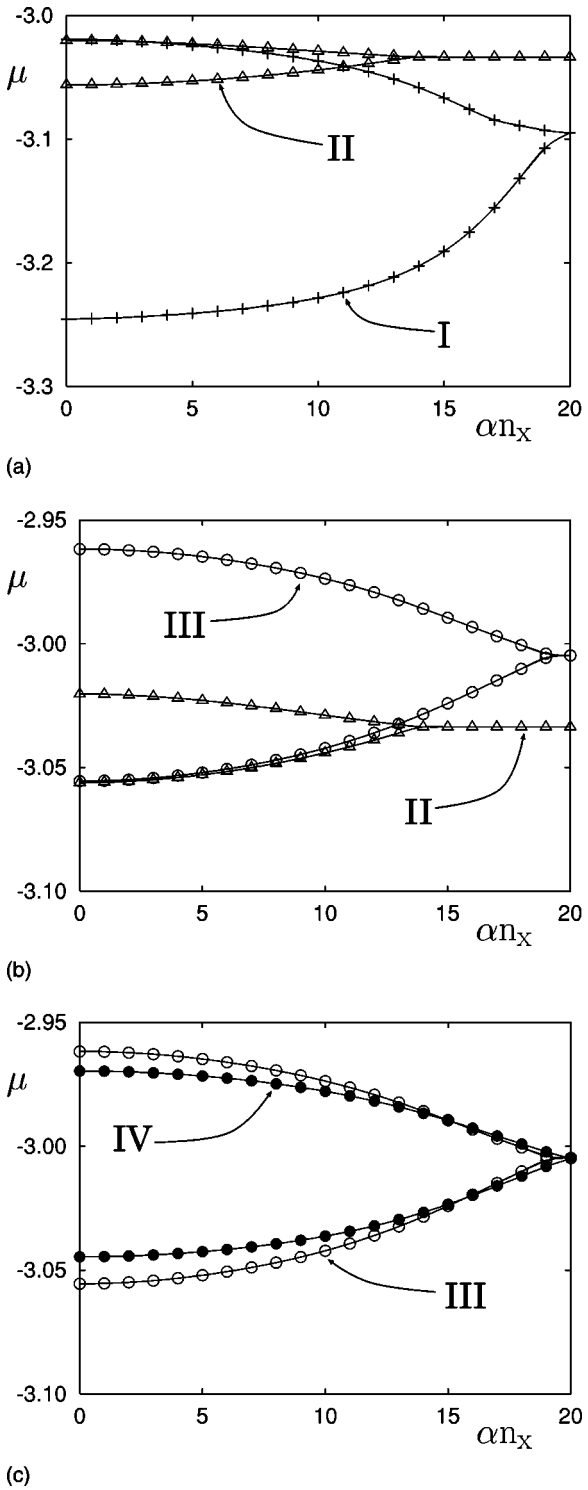

FIG. 2. Coexistence lines $\mu_x^{ij}(T,\alpha n_x)$ for $T=$const (see text). (a) Cases I and II, (b) Cases II and III, and (c) Cases III and IV (see Table I). Solid lines are intended to guide the eye.

where $\Omega^i\equiv\Omega[\boldsymbol{\rho}^i,T,\mu^{ij}]$ and i and j refer to particular morphologies [gas (g), bridge (b), or liquid (l)]. If $\Omega^i=\Omega^j$ is the absolute minimum of the grand potential at the intersection μ^{ij} for given values of T and αn_x, then $\mu_x^{ij}(T,\alpha n_x)\equiv\mu^{ij}$. Thus, the set of thermodynamic states

$$M=\{(\mu,\alpha n_x)|\mu_x^{gb}(T,\alpha n_x)<\mu<\mu_x^{bl}(T,\alpha n_x),T=\text{const}\} \tag{11}$$

represents the one-phase region of (sheared) bridge phases with which we shall be mainly concerned. For a given shear strain in the range $0<\alpha n_x<\alpha_> n_x$, the range of μ over which the bridge is the thermodynamically stable phase is specified by *M*. At $\alpha=\frac{1}{2}$ ($\alpha n_x=20$), where the substrates are maximally misaligned in the *x* direction, the bridge phase must vanish (i.e., the gas-bridge and liquid-bridge coexistence lines must merge at $\alpha=\frac{1}{2}$) on account of the symmetry of the film-substrate potential energy. Depending on the parameters other than μ and αn_x, the plots in Fig. 2 exhibit bifurcations at $\alpha_> n_x<20$. Hence, for $\alpha n_x>\alpha_> n_x$ the single line corresponds to $\mu_x^{gl}(T,\alpha n_x)$ common to coexisting gas and liquid phases. Inspection of the curve labeled II in Fig. 2(a) for $\alpha n_x>14$ indicates that gas is the thermodynamically stable phase in the range $-\infty<\mu\lesssim-3.035$ whereas liquid is stable over the range $-3.035\lesssim\mu<\infty$. Consequently, $\alpha_{tr} n_x \equiv \alpha_> n_x$ is the shear strain at which gas, liquid, and bridge phases coexist and therefore $T\equiv T_{tr}^{gbl}(\alpha_> n_x)$ is the associated shear-strain dependent triple-point temperature (see, for example, Fig. 9 in Ref. [27]).

Table I indicates that the curves of each pair plotted in Figs. 2(a)–2(c) differ only in one parameter (namely, ϵ_{fw}, n_z, or *T*). For example, curves I and II in Fig. 2(a) correspond to bridges of different lengths (n_z). One expects the longer bridge to be less stable against shear deformation, since work needs to be done on the bridge to stretch it. This notion can be quantified by introducing the ''area''

$$A_{1\Phi}=\int_0^{\alpha_> n_x}[\mu_x^{bl}(T,\alpha n_x)-\mu_x^{gb}(T,\alpha n_x)]d(\alpha n_x) \tag{12}$$

associated with the region of stability of the bridge phase given by Eq. (11). From Fig. 2(a) it is clear that $A_{1\Phi}$ for case II ($n_z=10$) is much smaller than $A_{1\Phi}$ for case I ($n_z=5$). Moreover, $\alpha_> n_x$ for case II is considerably less than $\alpha_> n_x$ for case I. Note also that for both cases the one-phase region is characterized by chemical potentials $\mu\in M$ *below* bulk saturation (i.e., $\mu<\mu^{\text{sat}}=-3$), which indicates that all phase transitions (i.e., gas-bridge, bridge-liquid, and gas-liquid) occur at chemical potentials below bulk saturation. The essential reason for this behavior is that the net attraction of the lattice gas by the entire substrate is sufficiently strong to support partial (gas-bridge) or complete (bridge-liquid or gas-liquid) condensation.

This scenario changes in Fig. 2(b) where now $\mu_x^{bl}(T,\alpha n_x)$ for case III is shifted to values exceeding those of bulk saturation (i.e., $\mu>\mu^{\text{sat}}=-3$, $\mu\in M$), except for the range $18<\alpha n_x\leqslant 20$. Notice also that for case III $\mu_x^{gb}(T,\alpha n_x)$ is nearly identical with its counterpart for case II up to the bifurcation $\alpha_> n_x=14$ of the latter. Hence, $A_{1\Phi}$ is considerably larger for case III than for case II. This can be rationalized in terms of the reduced attraction of the lattice gas by the weak stripes (see Table I). To understand this one has to realize that (partial) condensation of gas leading to the formation of a fluid bridge is promoted predominantly by the *strong* stripes on account of the short-range nature of fluid-substrate interactions. Therefore, since ϵ_{fs} remains unaltered between cases II and III, one expects $\mu_x^{gb}(T,\alpha n_x)$ to remain unaffected, as the plots in Fig. 2(b) confirm. Again on account of the short-range nature of fluid-substrate interactions, condensation of a bridge phase leading to the formation of a liquid is largely controlled by the *weak* stripes (i.e., by ϵ_{fw}). Since the latter are purely repulsive for case III (and therefore do not promote condensation at all), $\mu_x^{bl}(T,\alpha n_x)$ is shifted to chemical potentials exceeding μ^{sat}. In other words, the magnitude of $A_{1\Phi}$ is determined by the degree of heterogeneity of the substrate, a measure of which is the difference $\epsilon_{fs}-\epsilon_{fw}$.

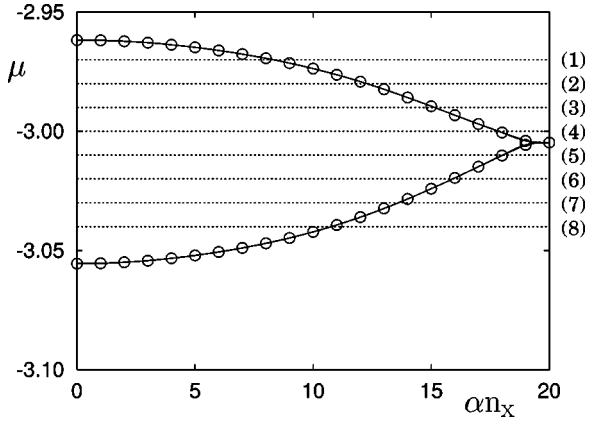

FIG. 3. As Fig. 2 for case III (see Table I). Dotted lines indicate paths of constant chemical potential (i.e., constant relative humidity) for which the mean density of bridge phases is plotted in Fig. 4.

Figure 2(c) demonstrates the effect of increasing temperature of the longer bridge from $T=1.20$ (case III) to $T=1.35$ (case IV). Over the range $0<\alpha n_x<15$ the warmer bridge is stable over a wider range of chemical potential. Above $\alpha n_x=15$ the opposite is true. The area $A_{1\Phi}$ is greater for case III, which indicates that the cooler bridge is the more robust.

B. Mean density of sheared bridge phases

To make contact with the experiment of Scherge *et al.* in Sec. IV we examine the variation in the mean density of the bridge $\overline{\rho}(\mu,T,\alpha n_x)$,

$$\overline{\rho}(\mu,T,\alpha n_x)=\frac{1}{\mathcal{N}}\sum_{i=1}^{\mathcal{N}}\rho_i(\mu,T,\alpha n_x), \tag{13}$$

along paths of constant *T* and μ [i.e., under constant relative humidity $\mu/\mu^{\text{sat}}\propto\ln(p/p^{\text{sat}})$] indicated by the dotted lines in Fig. 3. The corresponding $\overline{\rho}(\mu,T,\alpha n_x)$ is shown in Fig. 4, where we consider only thermodynamic states in the set *M* defined in Eq. (11). Since the shear strain at the intersection between a line of constant μ and either $\mu_x^{gb}(T,\alpha n_x)$ or $\mu_x^{bl}(T,\alpha n_x)$ (i.e., the envelope of *M*) depends on μ as shown in Fig. 3, the curves plotted in Fig. 4 vary in length. Moreover, $\overline{\rho}(\mu,T,\alpha n_x)$ is a monotonically increasing or decreasing function of αn_x, respectively, above or below some characteristic chemical potential μ_0 defined through

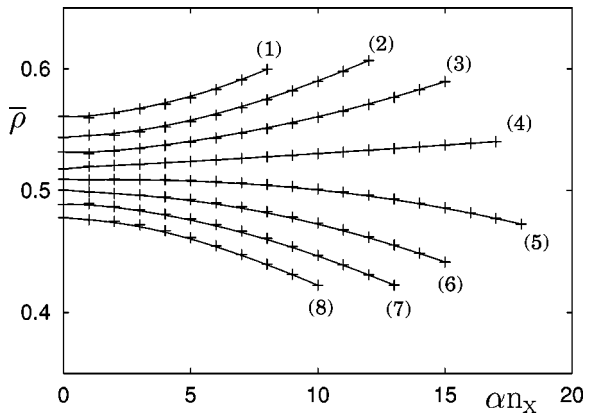

FIG. 4. Mean density $\overline{\rho}$ of bridge phase as function of shear strain αn_x for case III along paths of constant chemical potential identified in Fig. 3. Solid lines are intended to guide the eye. Curves end at intersection between $\mu=$const and coexistence lines limiting one-phase region of bridge phases in Fig. 3 (see text).

$$\left(\frac{\partial\overline{\rho}}{\partial(\alpha n_x)}\right)_{T,\mu}\Bigg|_{\mu=\mu_0}=0 \tag{14}$$

near the ''center'' of M [see Eq. (11)]. For case III, $\mu_0 \approx \mu^{\mathrm{sat}}=-3$. However, we emphasize that this approximate equality is fortuitous. In general, μ_0 depends on the parameters n_s, n_w, ϵ_{fs}, ϵ_{fw}, and T. Intuitively, the dependence of $\overline{\rho}(\mu,T,\alpha n_x)$ seems sensible. If, on the one hand, a bridge phase is sheared along paths of constant $\mu<\mu_0$, it must eventually coexist with a gas phase at the intersection between this constant μ and $\mu_x^{gb}(T,\alpha n_x)$ (see Fig. 3). Thus, the bridge phase must become more gaslike as the intersection is approached. Hence the mean density of bridge phases in the regime $\mu<\mu_0$ should decrease with increasing shear strain. If, on the other hand, a bridge phase is sheared at constant $\mu>\mu_0$, it must eventually coexist with a liquid phase where $\mu=\mu_x^{bl}(T,\alpha n_x)$. By the same logic one therefore expects the mean density of this bridge phase to increase with the shear strain.

The mean density is related to the shear stress through the Maxwell relation [30]

$$-\left(\frac{\partial\overline{\rho}}{\partial(\alpha n_x)}\right)_{T,\mu,\boldsymbol{n}}=\frac{1}{n_z}\left(\frac{\partial T_{zx}}{\partial\mu}\right)_{T,\alpha n_x,\boldsymbol{n}}, \tag{15}$$

where the vector $\boldsymbol{n}\equiv(n_x,n_y,n_z)$. Thus, from the plots in Fig. 4 and Eq. (15), T_{zx} must *increase* with increasing μ (i.e., with increasing relative humidity) over the range $\mu_x^{gb}(T,\alpha n_x)\leqslant\mu<\mu_0$ and *decrease* over the range $\mu_0<\mu \leqslant\mu_x^{bl}(T,\alpha n_x)$; for $\mu\equiv\mu_0$, T_{zx} is maximum. Moreover, this dependence of the shear stress on μ must hold regardless of the shear strain because $\overline{\rho}(\mu,T,\alpha n_x)$ is a monotonic function of αn_x for all thermodynamic states belonging to the set M, as the plots in Fig. 4 clearly show.

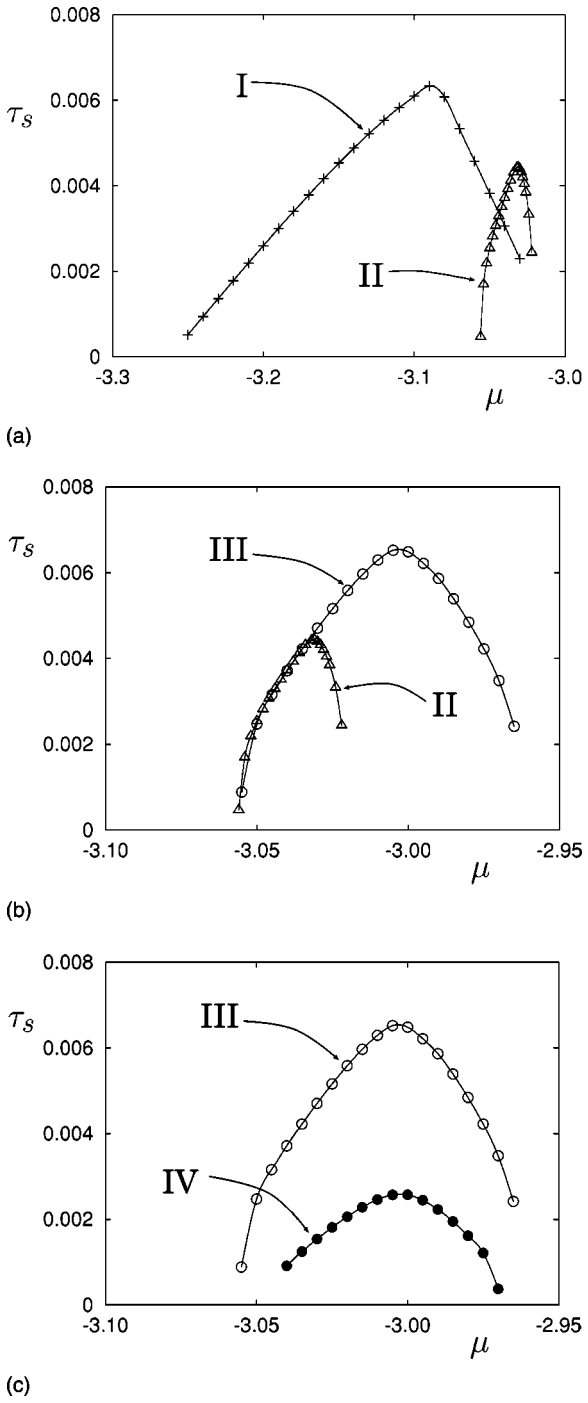

FIG. 5. Yield-strength versus chemical potential (i.e., relative humidity); (a) Cases I and II, (b) Cases II and III, and (c) Cases III and IV (see Table I).

C. Humidity dependence of yield strength

Since the yield strength τ_s is nothing but a particular value of T_{zx} (namely, its maximum, see Sec. III), we surmise on the basis of considerations in Sec. III B that $\tau_s(\mu)$ will increase and decrease with increasing μ (i.e., with increasing relative humidity) over the ranges $\mu_x^{gb}(T,\alpha n_x)\leqslant\mu<\mu_0$ and $\mu_0<\mu\leqslant\mu_x^{bl}(T,\alpha n_x)$, respectively, exhibiting a maximum at $\mu=\mu_0$. Plots of $\tau_s(\mu)$ in Fig. 5 confirm this. However, the

width of a curve as well as the location and height of its maximum depend on the parameters. Generally speaking, the width of $\tau_s(\mu)$ can be correlated with M [see Eq. (11), Figs. 2(a)–2(c)]. Therefore, the same arguments invoked above to rationalize the size and shape of one-phase regions of bridge phases can be employed here to understand variations in the width of $\tau_s(\mu)$.

According to its definition in Eq. (8), $\tau_s(\mu)$ is a measure of resistance of a bridge against its shear-induced destruction. This resistance is controlled essentially by the same factors that determine the magnitude of $A_{1\Phi}$ [see Eq. (12)]. However, we note that raising the temperature seems to reduce $\tau_s(\mu_0)$ more strongly [see Fig. 5(c)] than it reduces the magnitude of $A_{1\Phi}$ [see Fig. 2(c)]. This can be rationalized by observing that the density difference between regions of high(er) and low(er) density *within* a given bridge phase decreases with increasing T. In other words, the degree of heterogeneity of the bridge phase in the direction of the applied shear strain decreases with increasing temperature. Since this heterogeneity is the principal source of resistance of the bridge to lateral deformation, the yield strength must decline with temperature regardless of μ (that is, independently of the relative humidity).

D. Structure of sheared bridge phases

Additional insight can be acquired by examining the structure of the sheared bridge, which can be directly perceived in $\boldsymbol{\rho}$. A quantitative representation of the local density that minimizes the amount of information that must be displayed can be obtained by defining the set

$$S_> = \left\{ (x_i, z_i) \middle| \rho_i \equiv \rho(x_i, z_i) \geqslant \frac{1}{2} \right\} \tag{16}$$

of lattice sites at which the local density equals or exceeds $\frac{1}{2}$. These sites are indicated by dark gray (see Fig. 6). Complementing $S_>$ is the set

$$S_< = \left\{ (x_i, z_i) \middle| \rho_i \leqslant \frac{1}{2} \right\} \tag{17}$$

of lattice sites at which the local density is less than or equal to $\frac{1}{2}$ (denoted by white space in Fig. 6). The contour defined by

$$\mathcal{L} = S_> \cap S_< \tag{18}$$

is the line along which $\rho_i \equiv \frac{1}{2}$ and which separates the regions of ''high'' and ''low'' density.

For case II we consider these coarse-grained local density plots at $\alpha n_x = 12$ for three different values of μ: $\mu = -3.03$, $\mu = -2.98$, $\mu = \mu_0 \approx \mu^{\rm sat} = -3$. Figure 6(c) shows that for $\mu = \mu_0$ the width of the bridge in the x direction is constant along its length (z). The bridge appears to be ''stretched'' on account of the applied shear strain, that is, $\mathcal{L}$ is longer for the sheared bridge than for its unsheared counterpart. However, for μ below [see Fig. 6(a)] and above [see Fig. 6(b)] μ_0 the structure of the sheared bridge is distinctly different. The plot in Fig. 6(a) shows that the midsection of

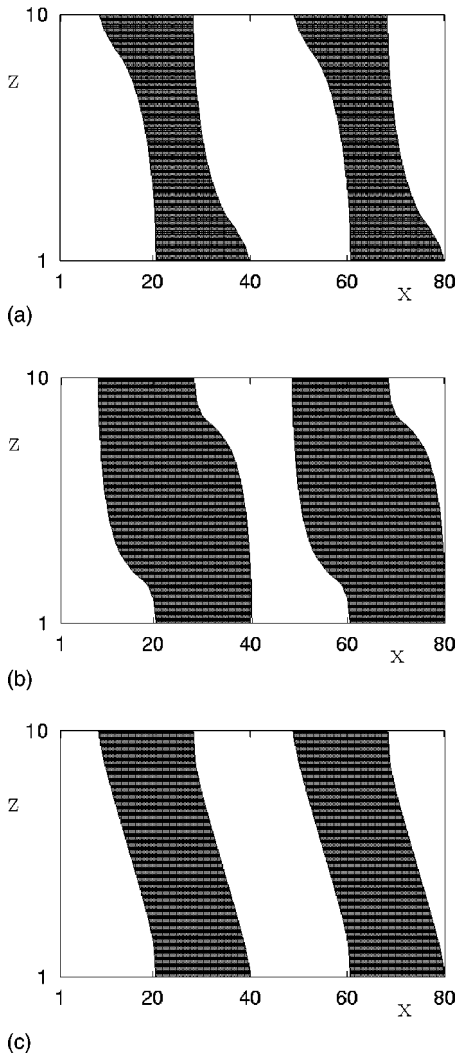

FIG. 6. The sets $S_>$ (gray area) and $S_<$ (white area) [see Eqs. (16) and (17)] separated by the line $\mathcal{L}$ [see Eq. (18)] for Case III at $\alpha n_x = 12$: (a) $\mu = -3.03$, (b) $\mu = -2.98$, and (c) $\mu_0 \approx \mu^{\rm sat} = -3$ (see text).

$S_>$ along the z direction is much narrower compared with the plot in Fig. 6(c). This is consistent with our earlier observation that $\overline{\rho}$ [that is, the mean density defined earlier in Eq. (13)] at $\mu < \mu_0$ is less than $\overline{\rho}$ at $\mu = \mu_0$ (see Figs. 3 and 4). By reducing its density the bridge phase at $\mu = -3.03$ maintains $\mathcal{L}$ approximately perpendicular to the direction of the applied shear strain, except for small regions in the vicinity of the substrates. A similar effect is observed for the bridge phase at $\mu = -2.98$ [see Fig. 6(b)], except that the density of the bridge increases with shear strain (see Figs. 3 and 4). Comparing Figs. 6(a) and 6(b) we note a curious and striking symmetry: $S_>$ *below* μ_0 is nearly identical with $S_<$ *above* μ_0 and vice versa.

Shear-induced structural changes in the bridge can be seen by comparing $\mathcal{L}$ for $\alpha n_x = 11$ with that for a slightly higher shear strain $\alpha n_x = 12$ in Fig. 7. For $\mu_0 \approx \mu = -3$ (that is, near the ''center'' of M), $\mathcal{L}$ shifts in the direction of the applied shear strain as the plot in Fig. 7(c) shows. The corresponding plots in Figs. 7(a) and 7(b) indicate that on ac-

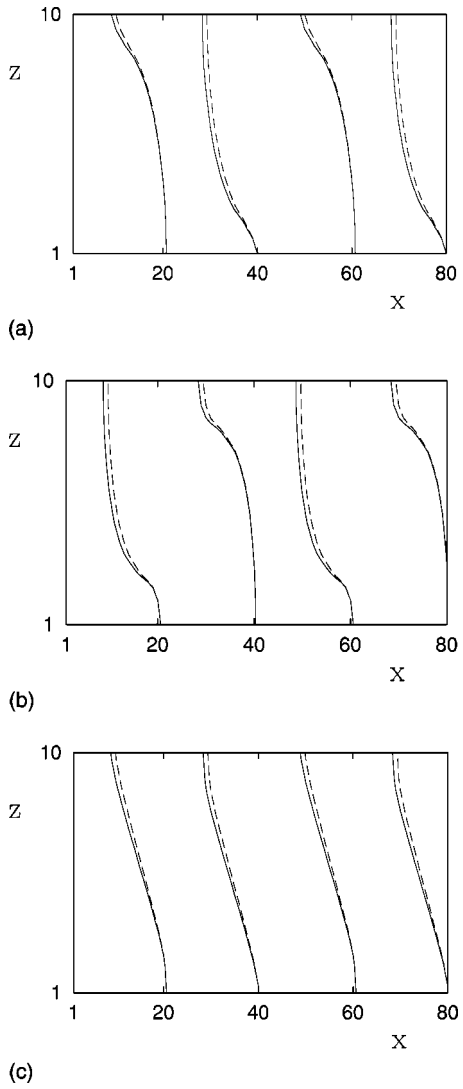

FIG. 7. As in Fig. 6, but only for the line $\mathcal{L}$ as a function of the shear strain: $\alpha n_x = 11$ (dashed line) and $\alpha n_x = 12$ (solid line).

count of the respective shear-induced decrease [see Fig. 7(a)] and increase [see Fig. 7(b)] in density only a part of $\mathcal{L}$ shifts upon increasing the shear strain. One notices furthermore from Fig. 5(b) that $\tau_s(\mu)$ is higher for $\mu_0 \approx \mu = -3$ compared with both $\mu = -2.98$ and $\mu = -3.03$, where only parts of $\mathcal{L}$ shift. Since $\tau_s(\mu)$ is the (maximum) change in the grand potential per unit area [see Eq. (7)] we conclude that by altering its density the bridge can compensate part of the work done by shearing it. This effect is qualitatively the same, regardless of whether the change in αn_x increases or decreases the density of the bridge.

IV. DISCUSSION AND CONCLUSIONS

Experimental studies of the effects of humidity on the force of friction on the macroscale [8,9,23] implicate liquid bridges on the nanoscale. However, the macroscopic thermodynamic treatment [8] of the phenomenon leaves open the question of the molecular mechanisms by which liquid bridges may give rise to friction. Using an ideal contact, we explore here the role of bridges in static friction at the nanoscale. Our model comprises a simple (spherically symmetric) fluid confined between two plane-parallel substrates decorated with weakly and strongly attractive stripes that alternate periodically in one transverse direction. It is the simplest model possessing the transverse heterogeneity necessary for the contact to sustain a shear stress. We describe the film approximately as a nearest-neighbor, mean-field cubic lattice gas. Previous investigations by us [25–27,29,30] have shown the model to give rise to bridge phases, although the mechanical properties of the bridges have not been systematically studied until now. In parallel with the experiment, we concentrate on the influence of chemical potential μ (analogous to humidity) on static friction. Specifically, we plot yield-strength curves (shear yield stress τ_s versus μ) and look at how they depend on other parameters of the model (i.e., distance n_z between the substrates, strength ϵ_{fw} of the ''weak'' stripe, and temperature T). We find that the width of the one-phase region of bridge phases (i.e., the range of μ over which the bridge phase is the thermodynamically stable phase) depends strongly on those other parameters. The yield-strength curve has a ''universal'' shape: as μ varies over the range of stability, τ_s exhibits a single maximum near the center of the range; τ_s is roughly symmetric about the maximum. This general dependence of τ_s on μ is intimately linked via a Maxwell relation to the variation of the mean density of bridge phases with the shear strain at constant chemical potential (i.e., constant relative humidity).

Variations of the yield-strength curve with alterations of n_z, ϵ_{fw}, and T can be correlated with the width of the one-phase region of bridge phases and their stability. The width of the one-phase region is controlled by the degree of chemical heterogeneity of the substrate, which depends on $\epsilon_{fs} - \epsilon_{fw}$, that is, the difference in strength of attraction of a lattice-gas molecule by the ''strong'' and ''weak'' stripes. Stability of the bridge phase, on the other hand, depends on the length of the bridge spanning the gap between the opposite ''strong'' stripes. The stability of a bridge also depends on its temperature. The higher T is, the more alike are high(er)- and low(er)-density regions of the bridge phase. Thus, ''warmer'' bridges are less heterogeneous in the direction of the applied shear strain. Since this heterogeneity is the source of resistance to the applied shear stress [27], the latter declines with increasing T.

The results of the model calculations are not strictly comparable with the experimental results of Scherge *et al.* [23], but several common trends are worthy of mention. Scherge *et al.* measured the force of friction between a 2-mm sapphire sphere and ''flat'' silicon surfaces as a function of humidity at several temperatures and at a constant *load*. In the case of the ''hydrophilic'' Si surface (which would be attractive to water molecules) they observe that friction (1) rises with humidity and at the lower temperatures studied may go through a maximum; (2) increases with decreasing temperature; and (3) rises with increasing relative humidity toward a maximum more rapidly at lower temperature than at higher temperature.

The experiment utilizes a macroscopic contact and thus

involves a distribution of sizes and shapes of nanoscopic contacts. Moreover, in the experiment the load is fixed rather than the separation between sphere and flat, whereas in the model the distance between the substrates of the single nanoscopic contact is kept constant rather than the normal stress (load per unit area). Nevertheless, in parallel with the experiment we find that (1) τ_s rises with increasing μ and can go through a maximum in the range of μ *below* saturation (see Figs. 4 and 5); (2) τ_s increases with decreasing T (see Fig. 5); and (3) τ_s rises with increasing μ toward a maximum more rapidly at lower T than at higher T (see Fig. 5). These similarities encourage us to believe that the model has essential elements in common with the real system and that with appropriate refinements the experiment and theory may together yield useful insight into the role of fluid bridges in friction.

ACKNOWLEDGMENTS

We are grateful for financial support from the Sonderforschungsbereich 448 ''Mesoskopisch strukturierte Verbundsysteme,'' which made possible an extended stay for one of us (D.J.D.) in the Stranski-Laboratorium für Physikalische und Theoretische Chemie, during which period this research was carried out. D.J.D. thanks Professor G. H. Findenegg of the Stranski-Laboratorium and also Professor S. Hess of the Institut für Theoretische Physik for their warm hospitality.

[1] F. P. Bowden and D. Tabor, *Friction and Lubrication* (Methuen, Oxford, 1956), Chap. 1.
[2] A. W. Adamson, *Physical Chemistry of Surfaces*, 3rd ed. (Wiley, New York, 1976), Chap. X.
[3] F. Heslot, T. Baumberger, B. Perrin, B. Caroli, and C. Caroli, Phys. Rev. E **49**, 4973 (1994).
[4] J.T. Burwell and E. Rabinowitz, J. Appl. Phys. **24**, 136 (1953).
[5] C. H. Scholz, *Mechanics of Earthquakes and Faulting* (Cambridge University Press, Cambridge, 1990), Chap. 2.
[6] J.H. Dieterich, Pure Appl. Geophys. **116**, 790 (1978).
[7] D. Severin and F. Musiol, Konstruktion **47**, 59 (1995).
[8] L. Bocquet, E. Charlaix, S. Ciliberto, and J. Crassous, Nature (London) **396**, 735 (1998).
[9] G. D'Anna, Phys. Rev. E **62**, 982 (2000).
[10] F. Restagno, L. Bocquet, T. Biben, and E. Charlaix, J. Phys.: Condens. Matter **12**, A419 (2000).
[11] K. J. Laidler, *Chemical Kinetics* (Harper & Row, New York, 1987), Chap. 4.
[12] H. T. Davis, *Statistical Mechanics of Phases, Interfaces, and Thin Films* (Wiley-VCH, New York, 1996), Chap. 7.
[13] T.A. Core, W.K. Tsang, and S.J. Sherman, Solid State Technol. **36**, 39 (1993).
[14] C. Gao, P. Dai, A. Homola, and J. Weiss, J. Tribol. **120**, 358 (1998).
[15] D.W.L. Tolfree, Rep. Prog. Phys. **61**, 313 (1998).
[16] P. Bönsch, D. Wüllner, T. Schrimpf, A. Schlachletski, and R. Lacmann, J. Electrochem. Soc. **145**, 1273 (1998).
[17] J.L. Wilbur, A. Kumar, E. Kim and G.M. Whitesides, Adv. Mater. **6**, 600 (1994).
[18] J.N. Israelachvili, *Intermolecular and Surface Forces*, 2nd ed. (Academic, London, 1992), Chap. 15.
[19] R.W. Carpick and M. Salmeron, Chem. Rev. **97**, 1163 (1997).
[20] *Fundamentals of Friction: Macroscopic and Microscopic Processes*, edited by I.L. Singer and H.M. Pollock (Kluwer, Dordrecht, 1991), Chap. VI.
[21] I.L. Singer, J. Vac. Sci. Technol. A **12**, 2605 (1994).
[22] J. Crassous, E. Charlaix, and J.L. Loubet, Europhys. Lett. **28**, 37 (1994).
[23] M. Scherge, X. Li, and J.A. Schaefer, Tribol. Lett. **6**, 215 (1999).
[24] M. Scherge and S. Gorb, *Biological Micro- and Nanotribology—Nature's Solutions* (Springer-Verlag, Berlin, 2001).
[25] M. Schoen and H. Bock, J. Phys.: Condens. Matter **12**, A333 (2000).
[26] H. Bock and M. Schoen, J. Phys.: Condens. Matter **12**, 1545 (2000).
[27] H. Bock and M. Schoen, J. Phys.: Condens. Matter **12**, 1569 (2000).
[28] H. Bock, M. Schoen, and D.J. Diestler, J. Phys.: Condens. Matter **13**, 4697 (2001).
[29] M. Schoen and D.J. Diestler, Phys. Rev. E **56**, 4427 (1997).
[30] H. Bock and M. Schoen, Phys. Rev. E **59**, 4122 (1999).
[31] P. Röcken and P. Tarazona, J. Chem. Phys. **105**, 2034 (1996).